HYDROGEN FUEL CELL & ENERGY STORAGE

Thermodynamic investigation of applying a thermoelectric generator to produce hydrogen in a multi-generation system

Mehrdad Mahmoudi[a] | Iraj Mirzaee[a] | Morteza Khalilian [a,*]

[a] Mechanical Engineering Department, Faculty of Engineering, Urmia University, Urmia, Iran

*Mechanical Engineering Department, Faculty of Engineering, Urmia University, Urmia, Iran.m.khalilian@urmia.ac.ir

Article Information

Article Type:
Research Article

Article History:

Received: 20 March 2023
Received in revised form 20 May 2023
Accepted: 15 June 2023
Published on line 20 June 2023

Keywords

Multigeneration system
Solar collector
Nanofluids
Thermoelectric generator
Hydrogen production

Abstract

In the near future, hydrogen is expected to become a significant fuel, greatly contributing to atmospheric air quality. So far, fossil fuels have dominated global hydrogen production. Pure hydrogen can be produced by electrolysis of water; however, it is an energy-demanding process. In this study, a novel multigeneration system is introduced using nanofluid in a solar system. The proposed system includes a quadruple effect absorption refrigeration cycle, a thermoelectric generator, a PEM electrolyzer, a vapor generator, and a domestic water heater. A parametric study was done to consider the effect of significant parameters on the system's efficiency. It was observed that the system generated 18.89 kW of power, and the collector energy and exergy efficiency were 82.21% and 80.48%, respectively. Furthermore, the results showed that the highest exergy destruction rate occurred in the solar system at the rate of 4461 kW. The energy and exergy COPs of the absorption chiller were discovered to be 1.527 and 0.936, respectively. The hydrogen production rate decreases by increasing the volume concentration of the nanoparticles, the solar radiation, and the figure of merit index.

Cite this article: Mahmoudi, M., Mirzaee, I., Khalilian, M. (2023). Thermodynamic investigation of applying a thermoelectric generator to produce hydrogen in a multi-generation system. DOI:10.22104/HFE.2023.6283.1262

Publisher:Iranian Research Organization for Science and Technology(IROST)
DOI: 10.22104/HFE.2023.6283.1262

NOMENCLATURE

A	Area (m^2)	$\dot{W}$	Net output power (kW)
C_p	Specific heat capacity (J/kgK)	x	The concentration of refrigerant in the solution
D	Collector diameter (m)	Z	Investment cost ($)
E	Energy input (kW)		
$\dot{E}x$	Exergy rate (W)	Subscripts	
ex	Exergy (J/kg)	0	Ambient
F_1	Collector efficiency factor	$1, 2, \ldots$	State points
F_R	Heat transfer factor	abs	Absorber
G	Solar irradiation (W/m^2)	ap	Aperture
h	Heat transfer coefficient (W/m^2K)	ARS	Absorption refrigeration cycle
J	Current density (A/m^2)	con	Condenser
k	Thermal conductivity (W/m K)	D	Destroyed
L	Collector length (m)	DWH	Domestic water heater
M	Molecular weight (kg/mol)	eva	Evaporator
$\dot{m}$	Mass flow rate (kg/s)	p	Pump
n_{cs}	Number of collectors in series	PEM	Proton exchange membrane
n_{cp}	Number of collectors in parallels	PTC	Parabolic trough collector
$\dot{N}$	Outlet flow rate of fluid x (kg/s)	r	Receiver tube
P	Pressure (bar)	TEG	Thermoelectric generator
$\dot{Q}$	Heat transfer rate (W)	vg	Vapor generator
Q_u	Useful energy gain	Greek Symbols	
S	Absorbed solar radiation		
T	Temperature (K)	η	Efficiency
U_L	Solar collector's overall heat loss coefficient	$\lambda(x)$	Water content at location x
V	Overpotential (V)	ρ	Density (kg/m^3)
w	Collector width (m)	ϕ	Concentration ratio

1. Introduction

Due to the increasing consumption and cost of non-renewable energy such as natural gas and electricity, the utilization of clean and renewable energy, like solar energy, geothermal energy, etc., has attracted the attention of researchers in recent years, resulting in the investigation of the possibility of using solar energy for cooling and heating in different places. Solar energy, an endless energy source for the planet, has always occupied a significant part of scientific research. The worldwide utilization of fossil fuels, particularly in Iran, has increased dramatically in recent years. In addition, the increasing trend of fossil fuel prices and their harmful environmental effects, such as pollution, increasing global temperature, and ozone layer destruction, has doubled the desire to use renewable and clean energies, such as solar energy. Since a large part of the energy used in the summer is dedicated to cooling residential and office buildings, leading to an energy crisis, solar chillers could be a suitable substitute for compression chillers with high electricity consumption. Therefore, absorption refrigeration systems have become popular in recent years from an energy and environmental point of view. Although the absorption chiller has a low performance coefficient, it can use low-temperature energy, such as solar energy, and also consumes much less electrical energy than the compression cycle, which consumes a significant amount of energy due to the presence of a compressor. Another advantage of the solar absorption refrigeration system is the simultaneity of the maximum solar radiation and maximum cooling load required for air conditioning.

Hydrogen can be generated in different ways, such as steam methane reforming, electrolysis, photo-electrocatalysis, and thermolysis. Unlike conventional alkaline technology, a proton exchange membrane (PEM) water electrolyzer has benefits like better dynamic operation efficiency, high voltage efficiency at higher current densities, and compact design [1]. Electricity can be generated through direct heat by using thermoelectric generators (TEG). TEGs have no moving parts, and therefore, they work silently. Moreover, they produce no emissions and have low operating costs [2].

The use of thermoelectric generators has been investigated in several studies. For example, Ketfi et al. [3] investigated the efficiency of a single-effect lithium bromide-water solar absorption refrigeration system with two types of solar collectors: vacuum tubes and flat plate collectors. They concluded that to provide 90 kilowatts of input heat to the heat generator, 225.5 square meters are needed if a flat plate collector is used, and 175.1 square meters are needed if a vacuum tube collector is used. Tapeh Kaboudy et al. [4] analyzed a single-effect absorption refrigeration cycle connected to solar flat plate and parabolic trough collectors in the city of Kish from an energy and exergy point of view. Their results showed that compared to the flat plate collector, the parabolic trough collector makes it easier to separate the ammonia refrigerant from the water absorber and improves the performance of the solar absorption refrigeration cycle by absorbing more solar radiation intensity and providing more thermal power in the heat generator. Shirazi et al. [5] conducted a parametric study of single, double, and triple-effect solar absorption chillers utilizing common solar collectors found on the market. They investigated single-effect absorption chillers with vacuum tube collectors and double-effect and triple-effect absorption chillers with parabolic trough collectors, Fresnel micro concentrators, and vacuum flat plates. Their results showed that the double-effect absorption chiller combined with the vacuum flat plate collector performs better in terms of both energy and economy in different climatic conditions.

Ozlu and Dincer [6] investigated a multigeneration cycle operated by solar energy. The proposed system produced electricity using the Kalina cycle and cooling via a four-stage absorption refrigeration cycle, and hydrogen was produced by applying a PEM electrolyzer. Bellos et al. [7] investigated the efficiency of a single-effect absorption system using four different types of solar collectors. The comparison results made it clear that the evacuated tube collector was more economical, and the parabolic trough collector led to a higher COP compared with the other collectors. Ratlamwala and Abid [8] evaluated the performance of three absorption chillers (single, double, and triple-effect absorption cycles) driven by solar PTC collectors using nanofluid as the working fluid. Results showed that the COP and exergy efficiency of the triple effect chiller was about 31.66% and 16% higher than the double effect cycle, respectively. Abid et al. [9] studied and compared four different absorption refrigeration cycles using solar energy from the thermodynamic point of view, and nanofluids were applied as the absorbent fluid in the collector. By taking into account different parameters, the outcomes showed that applying nanofluids led to higher collector efficiency. Moreover, it was found that the maximum amount of COP and lowest rate of exergy destruction were achieved for the quadruple effect absorption cycle [9].

Rahmani et al. [10] researched a solar-based absorption refrigeration cycle to provide the cooling effect of a building. They investigated the effects of applying magnetic nanoparticles in the collectors and nano refrigerants in the absorption chiller evaporator. Their results illustrated that 250 kJ/h more energy could be absorbed by the solar collectors by adding just 0.5 % nanofluid to the base fluid. Ma et al. [11] examined a combined solar single/double-effect absorption refrigeration system from thermodynamic and thermoeconomic points of view. The system was designed on a switching method based on the temperature of the solar heat source. The economic results proved that the payback period of the proposed system was 11.84 years.

Habibzadeh et al. [12] studied the effect of using SiO_2 and TiO_2 nanoparticles on the efficiency of the PTC solar collector in a multigeneration system. The results proved that the solar collector efficiency increases when the nanofluid is applied as the absorbent fluid. Moreover, the highest outlet collector was achieved by using Therminol VP1/SiO_2 nanofluid. Habibollahzade et al. [13] proposed a novel system including a PTC collector, TEG, Rankine cycle, and PEM. TEG replaced the condenser in the studied system to produce more power. According to the results, the rate of hydrogen generated by the system was 2.28 kg/h, and the achieved exergy efficiency was 13.29%. It was concluded that using TEG instead of a condenser increases the system's efficiency and decreases the total cost [13]. Assareh et al. [14] investigated the thermodynamic efficiency of two different renewable energy-based systems to produce hydrogen and electricity. Their design included an ORC cycle, a PEM unit, and a TEG. They found that when the geothermal system was applied as the heat source, the system produced 11.21% more hydrogen compared with when solar energy was used as the energy source. Musharavati et al. [15] proposed a novel combined cycle containing a solar pond, a PEM fuel cell, and a TEG. In their study, the TEG was used to completely recover the waste heat completely. According to the results, the system could generate 2288.8 kW of electricity, and 11.26% and 13.17 % energy and exergy efficiencies were obtained.

In summary, the previous studies showed the importance of clean cooling, power, and hydrogen production. Although a lot of investigations have been performed on solar-based absorption refrigeration systems, to the best of the authors' knowledge, no study has investigated the solar collector integration with a quadruple effect absorption refrigeration cycle, TEG unit, and PEM electrolyzer from an energy and exergy point of view. Moreover, the utilization of nanofluids in the solar-based multi-effect absorption refrigeration cycles is rarely studied in the literature. Therefore, in the present study, a solar-assisted quadruple effect absorption refrigeration system for cooling, a TEG as the power generation unit, and a PEM electrolyzer unit for hydrogen production are proposed and analyzed from an energy and exergy point of view. The TEG provides the power the PEM electrolyzer needs to produce hydrogen, and Al_2O_3/therminol-VP1 nanofluid is utilized in the solar collector as the heat absorbent. Different parameters were studied to determine their impact on the performance of the proposed cycle.

2. System description

Figure 1 depicts the schematic of the nanofluid-based solar-assisted integrated system. The system can be distributed into six parts. The first is the parabolic trough collector, which produces the required energy of the system. The second and third are the vapor generator (VG) unit and the domestic water heater (DWH) to produce the hot water. The fourth and fifth parts are the quadruple effect (QE) absorption refrigeration cycle to produce cooling and the TEG unit to supply the power needed by the electrolyzer. The sixth part is the PEM electrolyzer, which produces hydrogen by water electrolysis. Sunlight irradiates on the parabolic reflector, and after reflecting on the absorber, the nanofluid temperature in the absorption tube becomes high. The high-temperature nanofluid enters the VG and DWH to present vapor and hot water, respectively. After that, the nanofluid stream enters the VHTG of the QE to generate cooling. Since the nanofluid leaving the absorption refrigeration system is still hot, the TEG unit is used to recover the remaining excess heat from the nanofluid before entering the solar collector. Finally, the low-temperature nanofluid enters the PTC to be reheated.

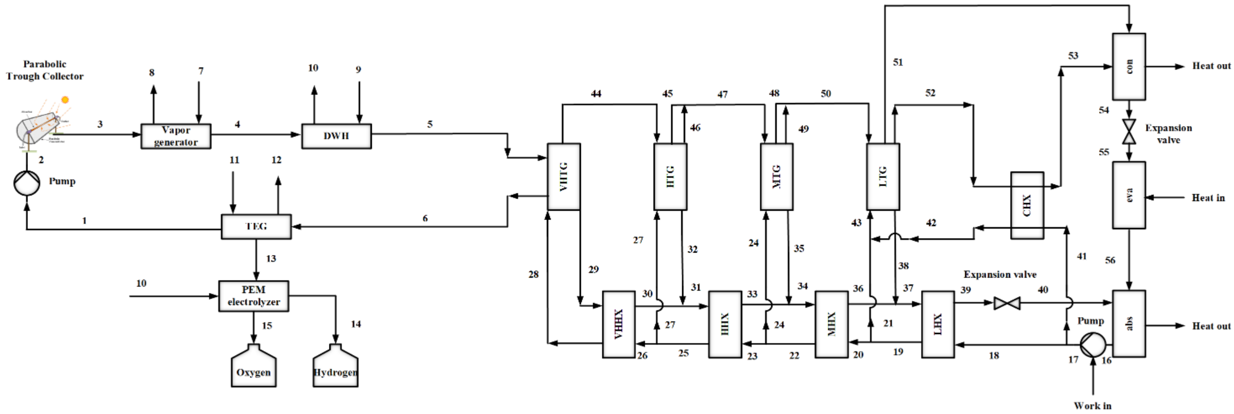

Fig1. Schematic of the nanofluid-based solar multigeneration system.

The working principle of the quadruple effect absorption refrigeration system is as follows: A strong ammonia water solution is evacuated from the absorber into the pump to increase its pressure. Then, it is apportioned into two flows. One flow enters low, medium, high, and very high-temperature heat exchangers to absorb heat from the returning stream from the generators. The first flow then moves into the VHTG to receive heat from the nanofluid to increase the temperature of the strong ammonia water solution to the boiling point. Boiling leads to the separation of the ammonia from the mixture. The ammonia vapor then enters the high, medium, and low-temperature generators to transfer the heat to the strong solution entering the generators. Lastly, the resulting low-heat ammonia vapor is discharged from the low-temperature generator in two streams: one stream directly enters the condenser, and the second stream goes into the condenser after proceeding through the condenser heat exchanger to give its heat to the second strong solution flow from the pump. In the condenser, the ammonia refrigerant distributes heat to the environment. After moving through the expansion valve, the refrigerant passes into the evaporator to gain heat from the environment. The weak solution flowing from the heat exchangers and ammonia refrigerant is mixed in the absorber and then leave the absorber in the form of a strong combined solution.

3. Modeling

First, this section presents the assumptions considered for accomplishing the simulation. Then, the methodologies and governing equations for the energy, exergy analysis, and the capital investment cost rate of each component are discussed.

Assumptions

Mathematical modeling and calculation of the integrated system are carried out based on the following assumptions:

- The pipe and heat losses are ignored.
- The system is analyzed based on the steady-state conditions, and the ammonia-water solution is considered steady.
- The heat is lost to the environment in the condenser and absorber.
- At the outlet of the condenser, the refrigerant is saturated liquid.
- At the outlet of the evaporator, the refrigerant is saturated vapor.
- At both ends of the expansion valves, the enthalpy is the same.
- Sudden changes in solar radiation have not been assumed in the analysis.

For the thermodynamic investigation of the studied system, the laws of mass conservation and the first and second laws of thermodynamics are used for each component of the proposed cycle. Each component can be used as a control volume for input and output flow, heat transfer, and work interaction [16].

$$\sum \dot{m}_i = \sum \dot{m}_e \tag{1}$$

$$\sum (\dot{m}\, x)_i = \sum (\dot{m}\, x)_e \tag{2}$$

$$\sum \dot{m}_i\, h_i - \sum \dot{m}_e\, h_e + \sum \dot{Q} - \sum \dot{W} = 0 \tag{3}$$

$$\sum \dot{Q}_k \left(1 - \frac{T_0}{T_k}\right) + \sum \dot{m}_i ex_i = \sum \dot{m}_e ex_e + \sum \dot{W} + \dot{E}x_{D,K} \tag{4}$$

The exergy of fluid flow is defined as follows:

$$ex = \left[\left(h_i - h_o\right) - T_o\left(s_i - s_o\right)\right] \tag{5}$$

Properties of nanofluids

In the present study, the aluminum oxide-Therminol VP1 nanofluid (Al_2O_3-Therminol VP1) is considered as the heat transfer fluid in the collector. The previous studies proved that applying nanofluids results in better thermophysical properties compared with the base fluids. Table 1 shows the thermodynamic properties of the studied nanoparticle:

Table 1. Properties of the studied nanoparticle [17].

Particle	ρ (kg/m³)	c_p (kJ/kgK)	k (W/mK)
Al_2O_3	3970	0.765	40

To identify the increase in heat transfer using nanofluids, it is necessary first to evaluate the thermophysical properties of nanofluids, such as thermal conductivity, density, viscosity, and specific heat capacity, which must be calculated in the design conditions.

The density of nanofluids (ρ) is presented as follows [18]:

$$\rho_{nf} = \varphi.\rho_{np} + (1-\varphi).\rho_{bf} \tag{6}$$

where φ is the nanoparticle volume concentration.

The specific heat capacity of nanofluid (c_p) can be expressed as follows [19]:

$$c_{p,nf} = \frac{\rho_{np}.\varphi.c_{p,np} + \rho_{bf}\,(1-\varphi).c_{p,bf}}{\rho_{nf}} \tag{7}$$

The thermal conductivity of nanofluid (k) is calculated using Maxwell's equation as follows [20]:

$$\frac{k_{nf}}{k_{bf}} = \frac{k_{np} + 2k_{bf} + 2\left(k_{np} - k_{bf}\right).(1+\beta)^3.\varphi}{k_{np} + 2k_{bf} - \left(k_{np} - k_{bf}\right).(1+\beta)^3.\varphi} \tag{8}$$

In equation (8) β is defined as the thickness of the nano-layer relative to the initial radius of the particle, and this parameter is usually considered to be 0.121]].

The dynamic viscosity of nanoparticle (μ) is estimated by the following relationship [17]:

$$\mu_{nf} = \mu_{bf}.\left(1 + 2.5\varphi + 6.5\varphi^2\right) \tag{9}$$

Parabolic trough solar collector

As parabolic collectors have a high acceptance angle, they can absorb both beam and scattered radiation. The nanofluid used as the absorbent fluid passes through the collectors, absorbs the heat of the solar energy, and is directly fed to other subsystems to generate electricity and other outputs. The actual useful energy absorbed in the collector is expressed as follows [22]:

$$Q_u = n_{cp} n_{cs} F_R A_{ap} [S - \frac{A_r}{A_{ap}} U_L (T_{r,i} - T_0)] \quad (10$$

where n_{cp} and n_{cs} are the number of collectors in parallel and series, respectively. Also, A_{ap} is the collector aperture area, A_r is the receiver area, and F_R is the heat removal factor. In addition, U_L expresses the heat loss coefficient of the entire collector. S shows the absorbed solar radiation and is defined as follows:

$$S = G_b \eta_r \quad (11$$

$$\eta_r = \gamma \tau_c \tau_p \alpha \quad (12$$

The areas of the aperture and receiver of the collector are:

$$A_{ap} = (w - D)L \quad (13$$

$$A_r = \pi D_0 L \quad (14$$

where w is the width, D is the external diameter of the glass cover, and L is the length of the collector. The following equations can be used to find F_R and F_l:

$$F_R = \frac{\dot{m} c_{p,c}}{A_r U_L} [1 - \exp(-\frac{A_r U_L F_l}{\dot{m} c_{p,c}})] \quad (15$$

$$F_1 = \frac{\frac{1}{U_L}}{\frac{1}{U_L} + \frac{D_{r,0}}{h_{fi}} + (\frac{D_{r,0}}{2k} \ln \frac{D_{r,0}}{D_{r,i}})} \quad (16$$

The input heat to the parabolic solar collector is expressed as follows:

$$Q_s = A_{ap} G_b \quad (17$$

The energy output of the solar collector is determined from the equations proposed by Duffy and Beckman [23] as follows:

$$\eta_{th,PTC} = \frac{Q_u}{Q_s} \quad (18$$

The input data required for the simulation of the collector is presented in Table 2.

Table 2. Input data considered in the simulation of the PTC collector.

Parameters	Unit	Value
SOLAR [24,25]		
Collector width	(m)	5.76
Collector length	(m)	99
Absorber outside diameter	(m)	0.07
Absorber inside diameter	(m)	0.066
Heat loss coefficient of the collector	$(W/m^{2\circ}C)$	3.82
The heat transfer coefficient in the inner side of the receiver	$(W/m^{2\circ}C)$	300
The receiver's thermal conductivity	$(W/m^{2\circ}C)$	16
Solar radiation intensity	$(W/m^{2\circ}C)$	850
Cover glazing transmissivity	-	0.96
Effective transmissivity	-	0.94
Receiver absorptivity	-	0.96
Correction factor for diffuse radiation	-	0.95
Nanoparticle volumetric concentration	$(\%)$	4

4. Thermoelectric generator

The energy balance formula for the TEG unit is exhibited as [26]:

$$\dot{Q}_{hot} = \dot{Q}_{cold} + \dot{W}_{TEG} \quad (19$$

where, $\dot{Q}_{hot}$ and $\dot{Q}_{cold}$ are the TEG's hot and cold side rate of heat transfer and $\dot{W}_{TEG}$ is the amount of the power produced by the TEG unit which can be calculated by:

$$\dot{W}_{TEG} = \eta_{TEG} \times \dot{Q}_{cold} \tag{20}$$

where η_{TEG} is the efficiency of the TEG unit and is defined as [27]:

$$\eta_{TEG} = \eta_{carnot}\left[\frac{(1+ZT_m)^{0.5}-1}{(1+ZT_m)^{0.5}-\left(\frac{T_{cold}}{T_{hot}}\right)}\right] \tag{21}$$

where, ZT_m is the figure of merit which is between 0.2 to 1.6 depending on the material property [28]. The Carnot efficiency and cold and hot temperatures are presented as:

$$\eta_{carnot} = \left(1-\frac{T_{cold}}{T_{hot}}\right) \tag{22}$$

$$T_{cold} = \frac{1}{2}\left(\frac{T_{11}+T_{12}}{2}\right) \tag{23}$$

$$T_{hot} = \frac{1}{2}\left(\frac{T_6+T_1}{2}\right) \tag{24}$$

The equations required for modeling the PEM unit are exhibited in Table 3.

Table 3. Equations required for the modeling of the PEM unit.

PEM [29]	
Electrical energy consumption	$\dot{E}_{electric} = JV$
Electrolyzer voltage	$V = V_0 + V_{act,c} + V_{act,a} + V_{ohm}$
Reversible equation	$V_0 = 1.229 - 0.00085(T_{PEM} - 298)$
Activation overpotential	$A_{act,i} = \frac{RT}{F}\sinh^{-1}\left(\frac{J}{2J_{0,i}}\right) = J_a^{ref}\exp\left(\frac{-E_{act,i}}{RT}\right), i = a,c$
Ohmic overpotential	$V_{ohm} = JR_{PEM}, R_{PEM} = \int_0^L \frac{dx}{\sigma[\lambda(x)]}, \lambda(x) = \frac{\lambda_a-\lambda_c}{D}x+\lambda_c$ $\sigma[\lambda(x)] = [0.5139\lambda(x)-0.326]\exp\left[1268\left(\frac{1}{303}-\frac{1}{T}\right)\right]$
Rate of produced H_2	$\dot{N}_{H_2,Out} = \frac{J}{2F} = \dot{N}_{H_2O,reacted}$

By using fundamental equations for all system types of equipment, the energy, exergy formulas, and cost functions for all types of equipment of the studied system can be determined as described in Tables 4 and 5.

Table 4. The cost functions applied for the different parts of the studied system.

Components	The cost functions [30-31]
PTC	$Z_{PTC} = 240 \times A_a$
Absorption chiller	$Z_{ARS} = 1144.3 \times (\dot{Q}_{eva})^{0.67}$
Vapor generator	$Z_{vg} = 1397 \times (A_{vg})^{0.89}$
PEM	$Z_{PEM} = 1000 \times \dot{W}_{pem}$
DWH	$Z_{DWH} = 130 \times (\frac{A_{DWH}}{0.093})^{0.78}$
TEG	$Z_{TEG} = 1500 \times \dot{W}_{TEG}$

Table 5. Energy and exergy equation of the proposed system.

Components	Energy equations	Exergy equations
PTC	$\dot{m}_2 h_2 + \dot{Q}_u = \dot{m}_3 h_3$	$\dot{E}x_{D,PTC} = \dot{E}x_{sun} + \dot{E}x_2 - \dot{E}x_3$
Vapor generator	$\dot{Q}_{vg} = \dot{m}_3 (h_3 - h_4) = \dot{m}_7 (h_8 - h_7)$	$\dot{E}x_{D,vg} = \dot{E}x_3 + \dot{E}x_7 - \dot{E}x_4 - \dot{E}x_8$
DWH	$\dot{Q}_{DWH} = \dot{m}_4 (h_4 - h_5) = \dot{m}_9 (h_{10} - h_9)$	$\dot{E}x_{DWH} = \dot{E}x_4 + \dot{E}x_9 - \dot{E}x_5 - \dot{E}x_{10}$
TEG	$\dot{Q}_{TEG} = \dot{m}_6 (h_6 - h_1) = \dot{m}_{11} (h_{12} - h_{11})$	$\dot{E}x_{TEG} = \dot{E}x_6 + \dot{E}x_{11} - \dot{E}x_1 - \dot{E}x_{12}$
PEM	$\dot{W}_{PEM} = \left(\dot{m}_{10} h_{10} - \dot{m}_{14} h_{14} - \dot{m}_{15} h_{15}\right)$	$\dot{E}x_{D,PEM} = \dot{E}x_{10} + \dot{W}_{PEM} - \dot{E}x_{14} - \dot{E}x_{15}$
ARC absorber	$\dot{Q}_{abs,ARS} = \dot{m}_{56} h_{56} + \dot{m}_{40} h_{40} - \dot{m}_{16} h_{16}$	$\dot{E}x_{D,abs,ARS} = \dot{E}x_{11} + \dot{E}x_{16} - \dot{E}x_1 - \left(1 - \frac{T_0}{T_{16}}\right)\dot{Q}_{abs}$
ARC condenser	$\dot{Q}_{con,ARS} = \dot{m}_{51} h_{51} + \dot{m}_{53} h_{53} - \dot{m}_{54} h_{54}$	$\dot{E}x_{D,con,ARS} = \dot{E}x_{51} + \dot{E}x_{53} - \dot{E}x_{54} - \left(1 - \frac{T_0}{T_{54}}\right)\dot{Q}_{con}$
ARC evaporator	$\dot{Q}_{eva,ARS} = \dot{m}_{55} \left(h_{56} - h_{55}\right)$	$\dot{E}x_{D,eva,ARS} = \dot{E}x_{10} - \dot{E}x_{11} + \left(1 - \frac{T_0}{T_{56}}\right)\dot{Q}_{eva}$
ARC VHTG	$\dot{Q}_{VHTG,ARS} = \dot{m}_{29} h_{29} + \dot{m}_{44} h_{44} - \dot{m}_{28} h_{28}$	$\dot{E}x_{D,VHTG,ARS} = \dot{E}x_{28} - \dot{E}x_{29} - \dot{E}x_{44} + \left(1 - \frac{T_0}{T_{44}}\right)\dot{Q}_{VHTG}$
ARC HTG	$\dot{Q}_{HTG,ARS} = \dot{m}_{44} h_{44} - \dot{m}_{45} h_{45}$	$\dot{E}x_{D,HTG,ARS} = \dot{E}x_{27} - \dot{E}x_{32} - \dot{E}x_{46} - \left(1 - \frac{T_0}{T_{32}}\right)\dot{Q}_{HTG}$
ARC MTG	$\dot{Q}_{MTG,ARS} = \dot{m}_{47} h_{47} - \dot{m}_{48} h_{48}$	$\dot{E}x_{D,MTG,ARS} = \dot{E}x_{24} - \dot{E}x_{35} - \dot{E}x_{49} - \left(1 - \frac{T_0}{T_{35}}\right)\dot{Q}_{MTG}$
ARC LTG	$\dot{Q}_{LTG,ARS} = \dot{m}_{50} h_{50} - \dot{m}_{51} h_{51}$	$\dot{E}x_{D,LTG,ARS} = \dot{E}x_{43} - \dot{E}x_{52} - \dot{E}x_{38} - \left(1 - \frac{T_0}{T_{38}}\right)\dot{Q}_{LTG}$
ARC Pump	$\dot{W}_{p,ARS} = \dot{m}_{16} \left(h_{17} - h_{16}\right)$	$\dot{E}x_{D,p,ARS} = \dot{E}x_{16} + \dot{W}_p - \dot{E}x_{17}$
COP	$COP_{en} = \frac{\dot{Q}_{eva}}{\dot{Q}_{VHTG} + \dot{W}_p}$	$COP_{ex} = \frac{\dot{E}x_{th,eva}}{\dot{E}x_{th,VHTG} + \dot{W}_p}$

5. Results and Discussion

Model validation

After describing all the needed equations to simulate the nanofluid-based parabolic trough collector as well as the other integrated systems, the conclusions of the investigated system are described by using different figures according to the varying parameters. EES software [32] was applied to perform all thermodynamic calculations, especially the thermal properties of the ammonia–H_2O solution. The cycle proposed by Ratlamwala and Abid [8] was used to validate the study's absorption system. The exergetic COP of the triple effect absorption system was validated when the evaporator temperature was assumed to be 13°C. The temperature of the generator varies between 127 to 177 °C. The comparative analysis in Figure 2 shows a reasonable agreement.

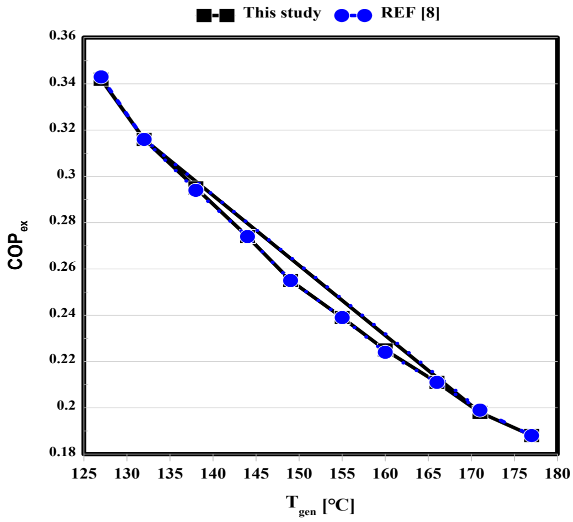

Fig2. A comparison of the exergetic COP of the triple effect absorption refrigeration system with Ref [8].

Results of parametric study

Table 6 depicts the overall performance of the proposed system under the basic defined conditions.

Table 6. The main results of the proposed multigeneration system.

Parameters	$\eta_{en,PTC}$ $(\%)$	$\eta_{ex,PTC}$ $(\%)$	Q_u (kW)	$\dot{Q}_{VG}$ (kW)	$\dot{Q}_{DWH}$ (kW)	$\dot{Q}_{cooling}$ (kW)	$\dot{W}_{TEG}$ (kW)	COP_{en}	COP_{ex}	$\dot{m}_{H2}$ (g/s)	Z $(\$)$
Results	82.21	80.48	10240	161.3	30.07	445.7	18.78	1.527	0.936	0.000742	69055

Figure 3 depicts the relative amounts of exergy destruction rate for the subsystems of the proposed multigeneration cycle. The figure shows that the solar collector's highest exergy destruction rate is 4461 kW. The primary reason for the solar collector's higher exergy destruction rate is the higher rate of the PTC's heat loss. The second and third highest exergy destruction rates occurred in the absorption refrigeration system and vapor generator, respectively. It can be inferred that the lowest exergy destruction rate among different subsystems refers to the domestic water heater.

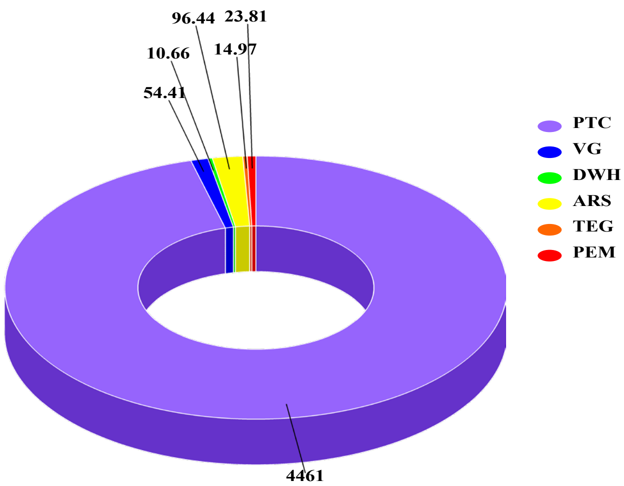

Fig 8. The share of each subsystem to the total amount of exergy destruction.

Figure 4 shows the changes in the hydrogen production rate and power produced by the TEG unit against the varying percentage of Al_2O_3 nanoparticles. According to the graphs, the increase in the Al_2O_3 nanoparticles percentage decreases the amount of power produced by the TEG unit and the amount of hydrogen produced by the PEM electrolyzer. The reason for the decrease is that when the nanoparticle percentage goes up, the outlet temperature of the collector decreases, reducing the amount of TEG efficiency. A reduction in the amount of TEG efficiency causes a decrease in the amount of power generated in the TEG unit. As the energy source of the PEM electrolyzer is the TEG unit, the decrease in the TEG power leads to a decrease in the amount of the system's generated hydrogen.

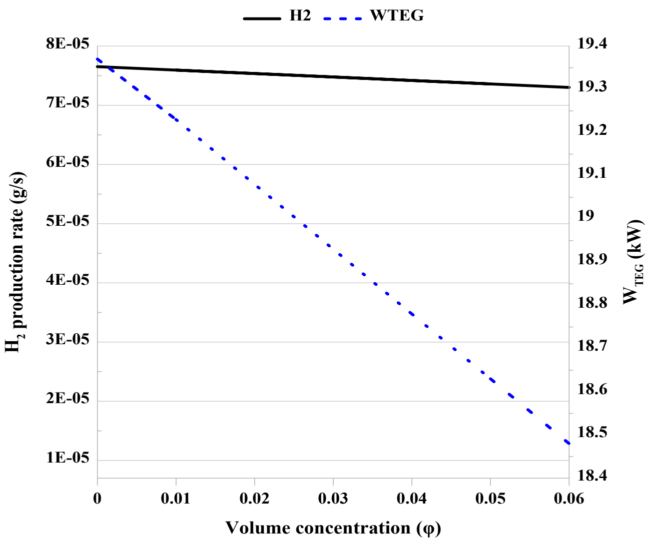

Fig 4. The effect of the nanoparticle volume concentration on the hydrogen production rate and generated power in the TEG unit.

Figure 5 shows the variation of power generation by TEG unit and hydrogen production rate of the system when the percentage of nanoparticles is fixed at 0.04. According to the results, when the solar radiation changes from 400 to 850 W/m^2, the generated hydrogen decreases from 0.003136 to 0.00066 g/s. The trend for the power produced by the TEG unit is different. By changing the amount of solar radiation, the amount of power first decreases from 79.38 to 0.3668 kW and then increases to 18.78 kW. The turning point happens between 600 to 650 K.

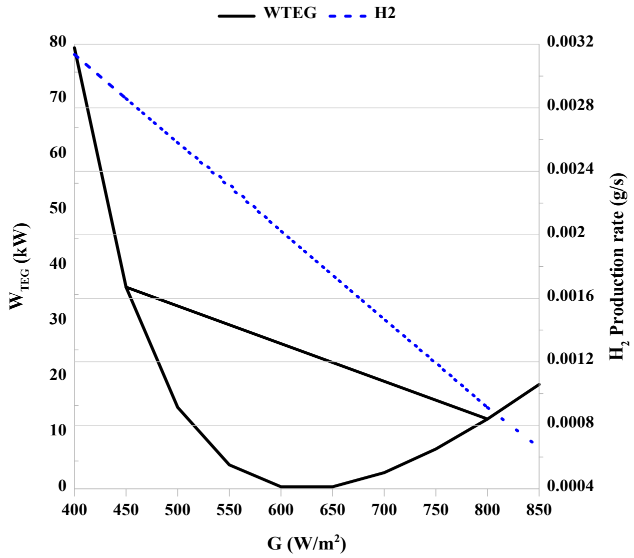

Fig 5. The effect of solar radiation on the power generation amount and the hydrogen production rate of the system.

Figure 6 exhibits the effect of changes in the very high-temperature generator load on the cooling content and energy and exergy COPs of the quadruple effect absorption refrigeration system. It is observed that by increasing the VHTG load from 290 to 340 kW, the rate of cooling generated by the system decreases from 446.2 to 396.3 kW. The main reason for the decrease in the cooling capacity is that an increase in VHTG capacity leads to a higher outlet ammonia vapor temperature, which enters the evaporator. Lower cooling capacity is produced when there is a small temperature distribution between the evaporator inlet and outlet. Moreover, the energy and exergy COPs are decreased by rising VHTG load. The reduction in the cooling load, with the rise in the VHTG capacity, negatively influences the system's efficiency, and for that, both COPs are reduced.

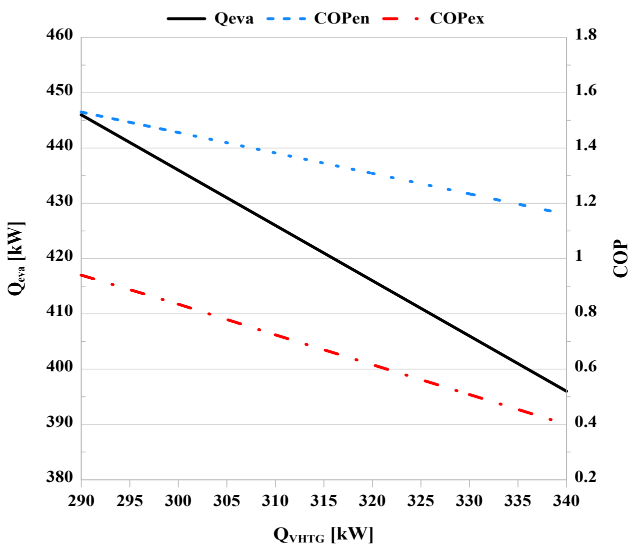

Fig 6. The effect of VHTG load on the cooling content and COPs of the absorption refrigeration system.

The effects of the increase in ambient temperature (T_0) on the absorption system are presented in Fig. 7. The results show the exergy COP rises from 0.56 to 0.92 when the ambient temperature varies from 270 to 290 K while the energy COP is constant at 1.53 for all ambient temperatures. The constant trend of the energy COP shows that the energy analysis results are not sensitive to environmental temperature variation. The increasing trend of the exergy COP indicates the lower exergetic heat loss from the system to the environment because of the lower temperature difference between the system and the environment.

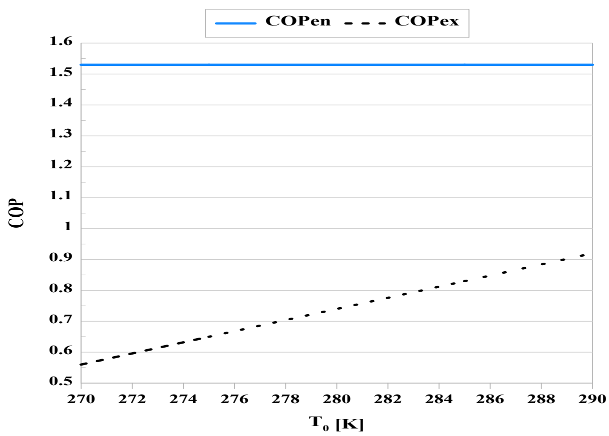

Fig 7. The effect of the concentration of the strong solution on the cooling content and COPs of the absorption refrigeration system.

The figure of merit (ZT) is a dimensionless parameter used to show the performance and efficiency of the TEG, and a ZT higher amount indicates the better performance of the TEG. The variation of hydrogen production amount and TEG output power with the figure of merit is depicted in Figure 8. According to the graphs, it can be inferred that a rising ZT leads to an increase in the amounts of TEG-generated power and the amount of hydrogen produced by the PEM electrolyzer. The amount of hydrogen produced by the system is directly linked to the rate of the generated power in the TEG unit. The reason for this relationship is that the TEG unit supplies the energy source of the PEM electrolyzer. Therefore, the more power generated in the TEG unit, the more hydrogen the PEM electrolyzer produces.

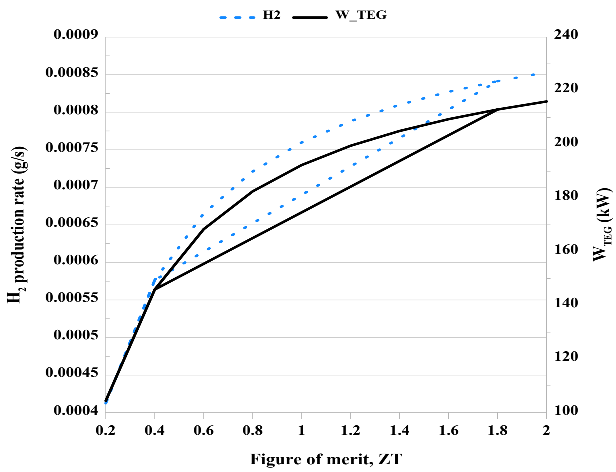

Fig 8. Effects of ZT on the hydrogen production amount and produced power of TEG unit.

Conclusion

The low thermal efficiency of solar systems can be improved by using nanofluids. In this study, thermodynamic analysis of a multigeneration system was investigated using EES software. A therminol VP1-AL_2O_3 nanofluid was used as the working fluid in the solar system. The multigeneration system includes a quadruple effect absorption refrigeration cycle for cooling generation, a TEG unit for power generation, a PEM electrolyzer for hydrogen production, a vapor generator for vapor, and a domestic water heater for hot water production. Different parameters were investigated, and the following results were obtained:

- The proposed system's first and second law efficiencies were 82.21% and 80.48%, respectively.
- The solar system possesses the highest amount of exergy destruction rate.
- Increasing the volume concentration of the nanoparticles decreases the power produced by the TEG unit and the hydrogen production amount.
- Increasing the solar radiation decreases the hydrogen production rate, but the power production amount first decreases and then increases.
- Increasing the temperature of the very high-temperature generator decreases the energy and exergy COPs of the system.
- Increasing the ambient temperature, energy COP remains constant while the exergy COP increases.
- Figure of merit increases lead to an increase in the amount of power generation and hydrogen production.

Refereces

[1] Ahmadi, P., Dincer, I. and Rosen, M.A., 2013. "Energy and exergy analyses of hydrogen production via solar-boosted ocean thermal energy conversion and PEM electrolysis", *International Journal of Hydrogen Energy*, 38(4), pp.1795-1805.

[2] Demir, M.E. and Dincer, I., 2017. "Development of a hybrid solar thermal system with TEG and PEM electrolyzer for hydrogen and power production", *International Journal of Hydrogen Energy*, 42(51), pp.30044-30056.

[3] Ketfi, O., Merzouk, M., Merzouk, N.K. and Metenan, S.E., 2015. "Performance of a Single Effect Solar Absorption Cooling System (Libr-H2O)", *Energy Procedia*, 74, pp:130-138.

[4] Tapeh Kaboudy, R., Suori, E. and Seyed Shams Taleghani S.A., 2016. "Investigation of thermodynamic analysis and exergy of a single effect solar absorption refrigeration cycle with parabolic collectors and the agent fluid of water and ammonia", 1st *International Conference on Mechanical Engineering and Aerospace*, University of Tehran, Tehran, Iran.

[5] Shirazi, A., Taylor, R.A., White, S.D. and Morrison G.L., 2016. "A systematic parametric study and feasibility assessment of solar-assisted single-effect, double-effect, and triple-effect absorption chillers for heating and cooling applications", *Energy Conversion and Management*, 114, pp:258-277.

[6] Ozlu, S. and Dincer, I., 2015. "Development and analysis of a solar and wind energy based multigeneration system", *Solar Energy*, 122, pp.1279-1295.

[7] Bellos, E., *Tzivanidis*, C. and Antonopoulos, K.A., 2016. "Exergetic, energetic and financial evaluation of a solar driven absorption cooling system with various collector types", *Applied Thermal Engineering*, 102, pp.749-759.

[8] Ratlamwala, T.A. and Abid, M., 2018. "Performance analysis of solar assisted multi-effect absorption cooling systems using nanofluids: a comparative analysis", *International Journal of Energy Research*, 42(9), pp.2901-2915.

[9] Bellos, E., *Tzivanidis*, C. and Antonopoulos, K.A., 2016. "Exergetic, energetic and financial evalua-

tion of a solar driven absorption cooling system with various collector types", *Applied Thermal Engineering*, 102, pp.749-759.

[10] Abid, M., Khan, M.S., Ratlamwala, T.A.H., Malik, M.N., Ali, H.M. and Cheok, Q., 2021. "Thermodynamic analysis and comparison of different absorption cycles driven by evacuated tube solar collector utilizing hybrid nanofluids", *Energy Conversion and Management*, 246, pp.114673.

[11] Rahmani, M., Nejad, A.S., Barzoki, M.F., Kasaeian, A. and Sameti, M., 2022. "Simulation of solar absorption refrigeration cycle with CuO nanofluid for summer cooling of a residential building", *Thermal Science and Engineering Progress*, 34, p.101419.

[12] Ma, H., Li, Q., Wang, D., Song, Q., Zhou, S., Wang, X. and Li, Y., 2022. "Operating performance and economic analysis of solar single/double-effect compound absorption refrigeration system", *Solar Energy*, 247, pp.73-85.

[13] Habibzadeh, A., Abbasalizadeh, Majid., Mirzaee, I., Jafarmadar, S. and Shirvani, H., 2023. "Thermodynamic Modeling and Analysis of a Solar and Geothermal-driven Multigeneration System Using TiO2 and SiO2 Nanoparticles", *Iranian (Iranica) Journal of Energy & Environment*, 14(2), pp.127-138.

[14] Habibollahzade, A., Gholamian, E., Ahmadi, P. and Behzadi, A., 2018. Multi-criteria optimization of an integrated energy system with thermoelectric generator, parabolic trough solar collector and electrolysis for hydrogen production. *International Journal of Hydrogen Energy*, *43*(31), pp.14140-14157.

[15] Assareh, E., Delpisheh, M., Farhadi, E., Peng, W. and Moghadasi, H., 2022. "Optimization of geothermal-and solar-driven clean electricity and hydrogen production multi-generation systems to address the energy nexus", *Energy Nexus*, 5, p.100043.

[16] Musharavati, F., Khanmohammadi, S., Nondy, J. and Gogoi, T.K., 2022. "Proposal of a new low-temperature thermodynamic cycle: 3E analysis and optimization of a solar pond integrated with fuel cell and thermoelectric generator", *Journal of Cleaner Production*, 331, p.129908.

[17] Borgnakke, C. and Sonntag, R.E., 2022. *Fundamentals of thermodynamics*. John Wiley & Sons.

[18] Duangthongsuk, W. and Wongwises, S. 2010. "An experimental study on the heat transfer performance and pressure drop of TiO_2-water nanofluids flowing under a turbulent flow regime", *International Journal of Heat and Mass Transfer*, 53, pp. 334-344.

[19] Ghasemi, S.E. and Ranjbar, A.A. 2016. "Thermal performance analysis of solar parabolic trough collector using nanofluid as working fluid: a CFD modelling study", *Journal of Molecular Liquids*, 222, pp. 15-166.

[20] Kasaeian, A.B. 2012. "Convection heat transfer modeling of Ag nanofluid using different viscosity theories", *IIUM Engineering Journal*, 13, pp. 1-11.

[21] Khanafer, K. and Vafai, K. 2011. "A critical synthesis of thermophysical characteristics of nanofluids", *International Journal of Heat and Mass Transfer*, 54, pp. 4410-4428.

[22] Yu, W. and Choi, S.U.S. 2003. "The role of interfacial layers in the enhanced thermal conductivity

of nanofluids: a renovated Maxwell model", *Journal of Nanoparticle Research*, 5, pp. 167-171.

[23] Kalogirou, S.A. 2013. *Solar energy engineering: processes and systems*: Academic Press.

[24] Duffie, J. and Beckman, W. 2006. *Solar Engineering of Thermal Processes. 2nd edition*: John Wiley and Sons. New Jersey.

[25] Keshtkar, M.M. and Khani, A.G., 2018. "Exergoeconomic analysis and optimization of a hybrid system based on multi-objective generation system in Iran: a case study", *Renewable Energy Focus*, 27, pp.1-13.

[26] Malik, M.Z., Musharavati, F., Khanmohammadi, S., Baseri, M.M., Ahmadi, P. and Nguyen, D.D., 2020. "Ocean thermal energy conversion (OTEC) system boosted with solar energy and TEG based on exergy and exergo-environment analysis and multi-objective optimization", *Solar Energy*, 208, pp.559-572.

[27] Aliahmadi, M., Moosavi, A. and Sadrhosseini, H., 2021. "Multi-objective optimization of regenerative ORC system integrated with thermoelectric generators for low-temperature waste heat recovery", *Energy Reports*, 7, pp.300-313.

[28] Chávez-Urbiola, E.A., Vorobiev, Y.V. and Bulat, L.P., 2012. "Solar hybrid systems with thermoelectric generators", *Solar Energy*, 86(1), pp.369-378.

[29] Abdolalipouradl M, Khalilarya S and Jafarmadar S., 2019 "Energy and exergy analysis of a new power, heating, oxygen and hydrogen cogeneration cycle based on the Sabalan Geothermal Wells", *International Journal of Engineering*, 32, pp:445–50.

[30] Yu, Z., Su, R. and Feng, C., 2020, "Thermodynamic analysis and multi-objective optimization of a novel power generation system driven by geothermal energy", *Energy*, 199, pp"117381.

[31] Ahmadi, P., Dincer, I. and Rosen, M.A., 2014, "Multi-objective optimization of a novel solar-based multigeneration energy system", Solar Energy, 108, pp:576-591.

[32] Klein, S.A. (2018) Engineering Equation Solver (EES) V9, F-Chart Software, Madison, USA.